NeuroImage 195 (2019) 333–339

Contents lists available at ScienceDirect

NeuroImage

journal homepage: www.elsevier.com/locate/neuroimage

Applicability and reproducibility of 2D multi-slice GRASE myelin water fraction with varying acquisition acceleration

Gerhard S. Drenthen [a,b,d], Walter H. Backes [a,b], Albert P. Aldenkamp [a,c,d], Jacobus F.A. Jansen [a,b,d,*]

[a] School for Mental Health and Neuroscience, Maastricht University Medical Center, P. Debyelaan 25, Maastricht, the Netherlands
[b] Department of Radiology and Nuclear Medicine, Maastricht University Medical Center, P. Debyelaan 25, Maastricht, the Netherlands
[c] Department of Behavioral Sciences, Epilepsy Center Kempenhaeghe, Sterkselseweg 65, Heeze, the Netherlands
[d] Department of Electrical Engineering, Eindhoven University of Technology, De Rondom 70, Eindhoven, the Netherlands

ARTICLE INFO

Keywords:
Myelin water fraction
T2 relaxometry
Reproducibility

ABSTRACT

Non-invasive quantification of the in vivo myelin content may provide valuable information regarding healthy maturation of the brain, as well as insights into demyelination of several neurological disorders. However, these scans are often long thereby limiting acquisition of large brain parts in clinically feasible acquisition times. Therefore, fast acquisition of whole brain myelin content is important. To avoid errors related to slice-selective pulses, most of the previous whole brain studies on myelin content relied on a 3D acquisition. However, multi-slice (2D) acquisition methods are often faster, and less susceptible to motion artifacts. Therefore, multi-slice approaches can be beneficial in a clinical setting.

We investigated the applicability and reproducibility of whole brain multi-slice GRASE myelin-water imaging with post-acquisition slice-profile correction in healthy volunteers (aged 25-32y). The applicability was evaluated using the agreement between the multi-slice GRASE and the reference method for myelin-water imaging, single-slice multi spin-echo (MSE) acquisition. Additionally, we assessed the effect of varying acquisition acceleration using parallel imaging on the reproducibility values.

First, the multi-slice myelin-water maps showed good agreement with the single-slice reference method, with a bias of at most 1.2% in absolute MWF values. Second, we found an average within-subject coefficient of variation (CoV) of 5.9% and an average intra-class correlation coefficient (ICC) of 0.90 for myelin-water estimation using a multi-slice GRASE sequence without parallel acceleration (scan time 14:06 min), while acquisition with a parallel acceleration factor of 2 resulted in a slightly worse average within-subject CoV of 6.4% and an average ICC of 0.83 at half the scan time. Hence, a multi-slice GRASE acquisition with parallel acceleration factor 2 and a scan time of 7:30 min still provides an excellent reproducibility.

1. Introduction

Myelin is a layered, fatty substance wrapped around the axons that is comprised of lipids and proteins. The myelin acts as an electrical insulator, accelerating the transport of electrical signals along the axons. Myelination is a vital process for a healthy neuronal maturation and development. Disruptions in the myelin content can have severe consequences and are related to several neurological disorders (Nave and Werner, 2014). Non-invasive quantification of the in vivo myelin content may provide valuable information regarding healthy maturation of the brain, as well as insights into demyelination of several neurological disorders.

Magnetic resonance imaging (MRI) is a technique which is sensitive to cerebral white matter abnormalities and has therefore extensively been used to investigate the myelin content. For example, diffusion weighted imaging (DWI), T1/T2 ratio imaging, and magnetization

Abbreviations: DWI, diffusion weighted imaging; UTE, ultra-short echo time; MWF, myelin water fraction; GRASE, gradient- and spin-echo; MSE, multi spin-echo; SVD, singular value decomposition; EPG, extended phase graph; NNLS, non-negative least squares; BA, bland-altman; CoV, coefficient of variation; RC, repeatability coefficient; ICC, intraclass correlation coefficient; SDws, within-subject standard deviation.

* Corresponding author. Department of Radiology and Nuclear Medicine, Maastricht University Medical Center, PO Box 5800, 6202, AZ, Maastricht, the Netherlands.

E-mail address: Jacobus.jansen@mumc.nl (J.F.A. Jansen).

https://doi.org/10.1016/j.neuroimage.2019.04.011
Received 14 November 2018; Received in revised form 20 March 2019; Accepted 3 April 2019
Available online 6 April 2019

transfer imaging have previously been used to assess the myelin content indirectly (Glasser and Van Essen, 2011; Hutchinson et al., 2010; van Buchem et al., 2001). While these methods provide markers that are related to the myelin content, they are not specific to the myelin content (Laule et al., 2007; Uddin et al., 2018a). Direct quantification of the myelin sheath can be achieved by ultra-short echo time (UTE) imaging (Sheth et al., 2016), however these sequences remain challenging on clinical MR systems due to hardware limitations (Seifert et al., 2017). Alternatively, myelin-water imaging using T2 relaxometry (Whittall and MacKay, 1989) or steady-state methods (mcDESPOT) (Deoni et al., 2008) have been applied to quantify the water components between the bilayers of the myelin sheath. These methods provide a specific marker of myelin content as water is an important component making up 40% of the total myelin volume (Alonso-Ortiz et al., 2015).

Using T2 relaxometry techniques, the relaxation of the MRI signal due to dephasing of water protons can be used to determine the myelin-water content. A number of different water compartments are present in brain tissue, each with a distinct T2 relaxation time. Water trapped between the bilayers of the myelin obeys a faster T2 relaxation ($15 < T2 < 40$ ms) compared to more freely moving water in the intra- and extracellular spaces ($80 < T2 < 100$ ms) and cerebrospinal fluid (CSF) ($T2 > 1000$ ms). Multi-echo T2 signal decay measurements are composed of a superposition of the signals from all water compartments. For myelin-water imaging it is relevant to determine the shortest T2, myelin-water, component (Alonso-Ortiz et al., 2015). Subsequently, myelin content can be quantified by taking the fraction of myelin-water signal to the total signal, the so-called myelin water fraction (MWF).

For MWF imaging to become more clinically feasible in a variety of populations and disorders, a rapid whole brain coverage with reproducible results is essential. Often, rapid whole brain coverage is achieved by accelerating image acquisition using parallel imaging techniques. However, these techniques introduce noise which can hamper the quality and consequently the reproducibility of the results. Currently, the impact of parallel imaging on the reproducibility is underdetermined. Moreover, whole brain MWF quantification has mainly focused on 3D sequences which do not suffer from imperfect slice profiles caused by slice-selective excitation pulses (Prasloski et al., 2012). However, 3D imaging techniques do, in general, require longer acquisition times compared to multi-slice (2D) techniques and are more susceptible to motion artifacts. Therefore, multi-slice imaging with a correction for imperfect slice profiles has previously been introduced as a method for fast MWF quantification (Akhondi-Asl et al., 2016; Guo et al., 2013; Kumar et al., 2016; Lebel and Wilman, 2010; Petrovic et al., 2015). Guo et al. and Kumar et al. avoided the imperfect slice profile in multi-slice imaging by using a refocusing slice thickness three times the size of the excitation slice. However, this limits the number of slices (about 5) that can be acquired at once. Instead, previous studies used a post-acquisition correction by estimating the imperfect slice profile (Akhondi-Asl et al., 2016; Lebel and Wilman, 2010; Petrovic et al., 2015).

In this study, we evaluate the use of multi-slice gradient- and spin-echo (GRASE) sequences with slice profile correction to quantitatively map the in vivo MWF. First, the applicability is evaluated using the agreement of the multi-slice GRASE and the reference method for myelin-water imaging, a single-slice multi spin-echo (MSE) acquisition. Subsequently, the reproducibility of the multi-slice GRASE MWF estimation, as well as the effect of accelerated image acquisition through parallel imaging is investigated.

2. Materials and methods

2.1. MRI data acquisition

Six volunteers (mean age 28y, range 25–32y, 3 males) were scanned on a 3.0 T unit (Philips Achieva, Best, the Netherland) using a 32-element head coil. Informed consent was obtained from all volunteers prior to inclusion. First, for anatomical reference, T1-weighted 3D turbo field echo images were acquired (repetition time (TR) = 8.2 ms, echo time (TE) = 3.7 ms, inversion time = 1010 ms, flip angle = 8°, voxel size 1 mm^3). As a reference (Alonso-Ortiz et al., 2015; Mackay et al., 1994), single transverse slice MSE images were acquired (TR = 3000 ms, 32 echoes with the shortest possible echo spacing for this sequence of 12 ms, range 12–384 ms, field of view 240 × 198 × 4 mm, matrix 160 × 132, voxel size 1.5 × 1.5 × 4 mm and 2 signal averages) for comparison to the multi-slice MWF images. For segmentation of major white matter fiber bundles, DWI was performed (TR = 7012 ms, TE = 74 ms, voxel size 2 mm^3, b value 1200 s/mm^2, 66 gradient directions and a single non-diffusion weighted b = 0 image, acquisition time 8:03 min).

To determine the MWF reproducibility of multi-slice GRASE imaging, for every volunteer two GRASE images were acquired (TR = 3000 ms, 32 echoes with 10 ms echo spacing, range 10–320 ms, EPI factor = 3, Turbo factor = 32, 26 slices, field of view 240 × 198 × 130 mm, matrix 160 × 132, voxel size = 1.5 × 1.5 × 4 mm) with and without parallel acquisition (sensitivity encoding, SENSE = 2), resulting in an acquisition time (TA) of 14:06 min and 7:30 min per GRASE scan, respectively. The relatively long TR warrants that T1 weighting is reduced substantially. To include variation related to repositioning, the volunteers went off the scan table after acquiring the first set of GRASE images (with and without parallel acquisition). After repositioning, the second GRASE set (with and without parallel acquisition) was acquired. The order in which the with/without parallel acquisition scans were acquired was switched after half of the volunteers were scanned to prevent a bias caused by the scanning order. For one volunteer, also multi-slice GRASE images were acquired with SENSE = 3 (TA: 5:06 min), 4 (TA: 4:12 min) and 8 (TA: 2:44 min) with the same spatial coverage.

2.2. Analysis

2.2.1. Preprocessing

For each volunteer, the GRASE and T1-weighted data were registered to the first echo image of the acquired first GRASE dataset (before repositioning) using the coregistration algorithm of the statistical parametric mapping (SPM12, https://www.fil.ion.ucl.ac.uk/spm/software/spm12/) toolkit (Friston et al., 2007). The diffusion MRI data was first corrected for head displacement, including B-matrix rotation, and eddy current induced geometric distortions using ExploreDTI v4.8.6 (Leemans et al., 2009). Subsequently, the DWI images were also registered to the native GRASE space.

A singular value decomposition (SVD) filter (Bydder and Du, 2006) was used to reduce noise in the multi-echo data, and a Gaussian kernel of 1.1 mm FWHM served to spatially smooth the GRASE and MSE images.

2.2.2. Regions of interest

Whole brain fiber tractography was performed using the diffusion tensor with a uniform seed point of 2 mm^3, a step size of 1 mm and a fractional anisotropy threshold of 0.2. Next, the fiber bundles of interest, the major and minor forceps, were extracted by selecting only those fibers going through the splenium and genu of the corpus callosum, respectively. Thereafter, the splenium and genu were manually delineated on these fiber bundles. Furthermore, using Freesurfer (version 5.3 (Fischl and Dale, 2000)), the corpus callosum, all white matter, cortical gray matter, caudate nuclei, thalamus and putamen were automatically segmented from the T1 weighted images. This resulted in 6 white matter regions of interest (ROIs) (major and minor forceps, the genu and splenium of the corpus callosum, the whole corpus callosum and all white matter) and 4 gray matter ROIs (cortical gray matter, caudate nuclei, thalamus and putamen).

2.2.3. Multi-exponential T2 relaxometry analysis

Multi-exponential analysis of the multi-echo data was performed using the non-negative least squares (NNLS) algorithm (Whittall and MacKay, 1989). To solve the NNLS, a basis set of 120 logarithmically spaced relaxation functions (T2 range 15–2000 ms) was used. The

algorithm was regularized using an additional minimal energy constraint that allows an increased misfit between 2 and 2.5% ($1.020 \leq \chi_{reg}/\chi_{min} \leq 1.025$) (Skinner et al., 2007).

Due to B1 inhomogeneities and imperfect slice profiles, the T2 relaxation does not behave as a pure exponential decay. To model the decay more accurately, the extended phase graph (EPG) was used to determine the T2 decay based on non-ideal refocusing pulses. The slice profile was estimated based on the Fourier transform of the slice-selective excitation pulse and, subsequently, the basis set was constructed by integrating the EPG decay profiles across the slice (Lebel and Wilman, 2010).

The B1 inhomogeneities were calculated by solving the multi-exponential problem for a range of possible B1 errors and subsequently selecting the B1 error that corresponds to the lowest residual of the fit. Determination of the B1 error is a noise sensitive procedure, therefore, to reduce possible errors due to noisy measurements, the multi-echo data were spatially averaged such that cubic voxels of approximately 4 mm^3 were obtained. Subsequently, the resulting B1 error map was smoothed using a Gaussian kernel of 2.3 mm FWHM. The spatial averaging and kernel size were selected, because the B1 map is expected to have smooth transitions without strong local changes. A B1 error range of 0.5–1.0 was used, which is equivalent to a flip angle range of 90–180°.

The MWF was calculated as the ratio of myelin-water associated T2 components (15–40 ms) to all T2 components (15–2000 ms). Previously, it was reported that the distribution of the MWF is skewed (Dayan et al., 2017; Kolind et al., 2012). Here we systematically observed that the MWF distribution in an ROI was (right-)skewed, and therefore we calculated the median to represent the MWF of the ROIs.

2.2.4. Statistical analysis

First, to investigate the applicability of multi-slice GRASE imaging, the MWF values estimated using the GRASE were plotted against the MWF values obtained with the single-slice MSE reference method. For this comparison, the MWF values estimated from the GRASE scan, obtained in the same session, were used.

Second, the reproducibility of the GRASE without parallel acquisition and the GRASE with an acceleration factor of 2 was evaluated using Bland-Altman (BA) analysis, the coefficient of variation (CoV), the repeatability coefficient (RC) and the intra-class correlation coefficient (ICC) (Wong et al., 2018).

In the BA analysis, for each ROI the bias between two methods as well as the 95% limits of agreement (LoA) are determined, where it is expected that these limits include 95% of the differences between two measurements of the methods. A one-sample *t*-test was used to test whether the bias between scan sessions was significantly different from zero. Furthermore, BA plots were created to inspect the agreement between the two methods visually. The CoV was determined as the within-subject standard deviation (SD_{ws}) relative to the overall mean for all subjects. The RC was defined as $1.95 \times \sqrt{2} \times SD_{ws}$, and provides a bound for the difference between two measurements for 95% of the observations. An ICC was calculated using a 1-way random model. The ICC can be interpreted as the fraction of total variance to the variance related to biological variation. An ICC of >0.60 is considered to be good reproducible (Cicchetti, 1994).

Last, the effect of further acceleration was assessed in a single volunteer. The MWF values obtained using the scans without parallel acceleration from the first session are compared to those from the scans with acceleration factors of 2, 3, 4 and 8 from the second session, using a BA analysis.

2.2.5. Image quality

To estimate the level of noise in the GRASE images with varying acceleration factors, the spatial variation, the signal-to-noise ratio (SNR_{raw}) of the raw images, and the SNR of the multi-exponential fits (SNR_{fit}) were calculated. The spatial variation was defined as the standard deviation of MWF values in the relatively homogeneous splenium. Since a multi-channel head coil was used, the calculation of the SNR_{raw} is not straightforward. For such cases, Wu et al. proposed a general framework for assessing SNR_{raw}, calculating the noise as mean of the background (Wu et al., 2010). Therefore, the SNR_{raw} was estimated as the mean signal obtained from a relatively homogeneous region of interest in the splenium (TE = 10 ms image) divided by the mean signal of the noise, measured in the noise regions of the air. The SNR_{fit} was estimated as the mean signal of the splenium (TE = 10 ms image) divided by the standard deviation of the fit residuals (Macmillan et al., 2011).

3. Results

3.1. Applicability

To investigate whether the multi-slice acquisition yields similar results compared to the reference method for MWF estimation, the single-slice reference MWF maps were compared to the corresponding slice in the multi-slice GRASE MWF maps. Due to variations in slice positioning, not all ROIs are available in all of the subjects. In Fig. 1, the agreement of the GRASE and reference MSE MWF estimation is shown. On average the MWF values reported using the GRASE are approximately higher by 0.9% absolute MWF values compared to the MSE. Only the MWF in the cortical gray matter is found to be lower using the GRASE. When comparing the MSE to the GRASE with an acceleration factor of 2, a comparable bias of 0.8% absolute MWF values is observed.

3.2. Reproducibility

The LoA and reproducibility measures of the GRASE MWF estimation, as well as the mean and between-subject standard deviation of the MWF for both measurements, are shown in Table 1 for an acceleration factor of 1, and in Table 2 for an acceleration factor of 2. The ICC for both acceleration factor 1 and 2 is indicative of a good reproducibility. None of the ROIs showed a bias between the measurements that was significantly different from 0 ($p > 0.05$).

Furthermore, the BA plots are shown in Fig. 2. The mean LoA for both acceleration factors are added for visualization.

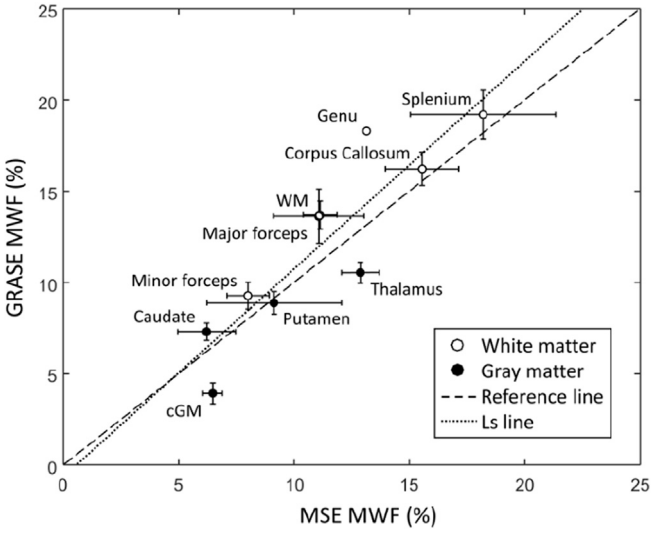

Fig. 1. The relation of the MWF values obtained using the reference MSE sequence, and the multi-slice GRASE sequence without parallel acceleration. The dashed line represents the line of equality, and the dotted line is a least-squares fit through the data points added for visualization. Note that the Genu is only available in one subject. Error bars depict 1 standard error. MWF, myelin-water fraction; WM, white matter; cGM, cortical gray matter; Ls, least-squares.

Table 1
Mean and standard deviation of the MWF values in the ROIs are shown for the first and second GRASE measurement (indicated by 1 and 2), both performed with an acceleration factor of 1. Additionally, the LoA and reproducibility measures are shown for each ROIs, as well as a mean of all ROIs. CC, corpus callosum; WM, white matter; cGM, cortical gray matter; ROI, region of interest; MWF, myelin-water fraction; LoA, limits of agreement; RC, repeatability coefficient; CoV, coefficient of variation; ICC, intra-class correlations coefficient.

	Acceleration factor 1					
ROI	MWF		LoA	RC	CoV (%)	ICC
	1	2				
White matter						
Genu	14.8 ± 2.1	14.5 ± 2.9	−3.9; 3.3	3.2	6.8	0.94
Splenium	20.0 ± 2.0	19.7 ± 3.4	−3.1; 2.5	2.1	3.3	0.87
Major forceps	14.0 ± 1.9	14.4 ± 2.7	−1.8; 2.4	1.3	2.9	0.94
Minor forceps	10.7 ± 1.7	10.2 ± 1.6	−1.2; 1.5	1.1	3.4	0.96
CC	16.8 ± 1.7	16.3 ± 2.2	−2.9; 2.0	2.1	4.7	0.89
WM	13.7 ± 1.5	13.6 ± 1.7	−1.8; 1.6	1.3	3.5	0.93
Gray matter						
cGM	5.0 ± 1.1	5.5 ± 1.4	−1.3; 2.1	1.9	10.2	0.82
Caudate nuclei	6.9 ± 1.0	6.8 ± 1.8	−2.5; 2.4	1.9	9.9	0.82
Thalamus	10.5 ± 1.5	10.5 ± 2.0	−2.4; 2.4	1.7	6.0	0.90
Putamen	7.5 ± 1.1	7.8 ± 1.7	−2.6; 3.1	2.1	9.8	0.71
Mean			−2.4; 2.3	1.9	6.1	0.88

Table 2
Mean and standard deviation of the MWF values in the ROIs are shown for the first and second GRASE measurements (indicated by 1 and 2), both performed with an acceleration factor of 2. Additionally, the LoA and reproducibility measures are shown for each ROIs, as well as a mean of all ROIs. CC, corpus callosum; WM, white matter; cGM, cortical gray matter; ROI, region of interest; MWF, myelin-water fraction; LoA, limits of agreement; RC, repeatability coefficient; CoV, coefficient of variation; ICC, intra-class correlations coefficient.

	Acceleration factor 2					
ROI	MWF		LoA	RC	CoV (%)	ICC
	1	2				
White matter						
Genu	14.5 ± 2.9	15.4 ± 1.5	−3.6; 3.6	3.0	6.1	0.78
Splenium	19.7 ± 3.4	18.8 ± 2.4	−2.3; 2.6	1.7	2.8	0.92
Major forceps	14.4 ± 2.7	14.0 ± 2.1	−2.7; 3.4	1.5	3.4	0.94
Minor forceps	10.2 ± 1.6	10.5 ± 1.1	−0.8; 2.2	2.4	7.1	0.76
CC	16.3 ± 2.2	16.7 ± 2.1	−4.1; 4.0	3.1	6.8	0.68
WM	13.4 ± 1.4	13.5 ± 1.3	−2.0; 2.1	1.6	4.4	0.85
Gray matter						
cGM	5.0 ± 1.0	5.4 ± 0.7	−2.4; 2.6	1.1	7.7	0.87
Caudate nuclei	7.2 ± 1.9	7.4 ± 2.0	−0.8; 1.6	1.9	9.3	0.85
Thalamus	10.0 ± 1.7	10.2 ± 1.0	−2.3; 2.7	1.9	6.7	0.77
Putamen	7.3 ± 1.4	7.5 ± 1.9	−3.6; 3.9	2.6	12.6	0.58
Mean			−2.5; 2.9	2.1	6.7	0.80

3.3. Image quality

The MWF maps of one subject are shown in Fig. 3 for the various acceleration factors. The spatial variation of the MWF values in the splenium increases for increasing acceleration factors (Fig. 4A). Up to factor 4, white matter and gray matter can still be distinguished to some extent.

The SNR_{raw} decreased for an increasing acceleration factor (Fig. 4B). Furthermore, the SNR_{fit} shows a similar decrease for acceleration factors up to 4 (Fig. 4C). Thereafter, for an acceleration factor of 8, a very steep drop in SNR_{fit} is observed, indicating a steep reduction in the accuracy of the fits.

3.4. Further acceleration

The effect of an increased acceleration factor is shown in Fig. 5, where the MWF values estimated from scans with varying acceleration factors are shown with respect to no parallel acceleration. The bias and LoA are also plotted in the figures.

4. Discussion

Initial MWF research has mainly focused on slow single-slice MSE acquisitions. Recently, methods that allow a whole brain coverage in clinically applicable scan times have emerged (Nguyen et al., 2016; Prasloski et al., 2012). Most of these whole brain methods are performed using a 3D acquisition mode. While this prevents distortions from slice-selective excitation pulses, scanning time is often relatively long and subject motion can corrupt the acquired 3D image. In this study, we have shown the applicability and reproducibility of MWF estimation using fast whole brain multi-slice GRASE imaging with post-acquisition slice-profile correction for varying acceleration factors using parallel imaging.

When we consider not only the parallel acceleration techniques but also the image resolution and FOV, the multi-slice GRASE sequence proposed in this study is roughly twice as fast compared to the 2D CPMG sequence proposed by Akhondi-Asl et al. (2016), as well as other 3D GRASE methods (Faizy et al., 2018; Ocklenburg et al., 2018; Prasloski et al., 2012; Uddin et al., 2018b). Although, it should be noted that compared to 3D alternatives the coverage of multi-slice GRASE is reduced by 20% due to the slice gap of 1 mm.

4.1. Applicability

The MWF values obtained with the multi-slice GRASE sequence are generally in good agreement with those estimated with the reference MSE sequence, showing a slight bias between the two methods of at most 0.9% in absolute MWF. Magnetization transfer effects introduced by the slice-selective excitation pulses likely have an influence on the determination of the MWF (Akhondi-Asl et al., 2016). Slice-selective pulses cause off-resonance excitation of bound hydrogen protons (i.e. macromolecules) in neighboring slices. The magnetization of these macromolecules exchanges with the more freely moving proton pool, subsequently decreasing its visibility and the pertaining signal. This effect could have a direct consequence on the MWF, as the myelin content is determined relative to the total signal. A decrease in signal could artificially increase the apparent MWF, resulting in a (slightly) higher MWF in multi-slice GRASE sequences compared to the reference MSE sequence. However, a previous study showed that for MSE, the signal of the myelin-water pool decreases even more due to magnetization transfer effects, subsequently lowering the MWF (Vavasour et al., 2000). Therefore, the exact role of the magnetization transfer effects on the reported bias of the multi-slice GRASE relative to the reference method remains unclear. Previously, two studies investigated the agreement between a 3D GRASE and 3D MSE sequence and showed excellent agreement (Ljungberg et al., 2017; Prasloski et al., 2012). Interestingly, in this study the cortical gray matter and thalamus show a higher MWF value using the MSE sequence. This

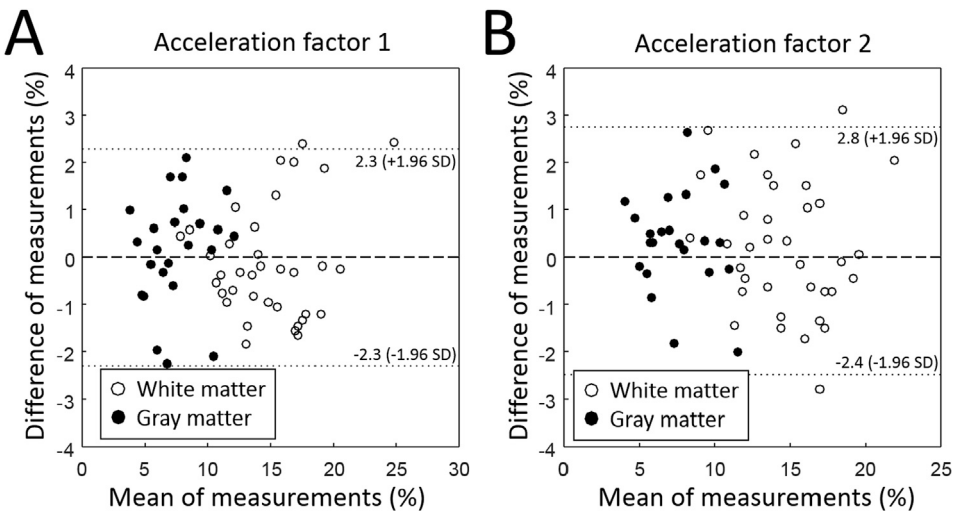

Fig. 2. Bland-Altman plots for the MWF values obtained using acceleration factors 1 and 2. The dashed line represents the x-axis, and the dotted lines shows the mean limits of agreement between the measurements. MWF, myelin-water fraction; SD, standard deviation.

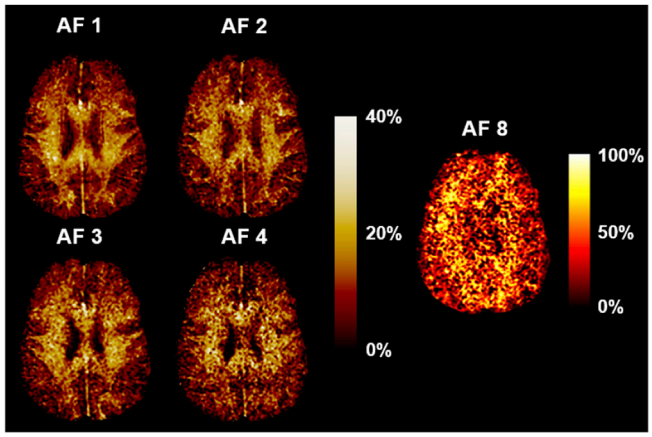

Fig. 3. Transverse MWF maps estimated from the multi-slice GRASE sequence for varying acceleration factors, 1 up to 8. Note that the MWF values for acceleration factor 8 ranges from 0 to 100%. MWF, myelin-water fraction; AF, acceleration factor.

aberrant behavior could be caused by flow artifacts, since it was previously found that the MSE is affected by flow artifacts differently than the 3D GRASE sequence (Prasloski et al., 2012). Further differences between the two methods could be caused by the differences in echo spacing, where the MSE sequence had an echo spacing of 12 ms (the shortest possible on our clinical system), the GRASE sequence that was used here had a shorter, and more ideal, echo spacing of 10 ms.

4.2. Reproducibility

The reproducibility of MWF estimation has a direct implication on the applicability in clinical studies. In the current study, we found a within-subject CoV of 6.1% (range 2.9–10.2%) and an ICC of 0.88 (range 0.71–0.96) for MWF estimation using a multi-slice GRASE sequence without parallel acceleration. Acquisition with an acceleration factor of 2 resulted in comparable values, a within-subject CoV of 6.7% (range 2.8–12.6%) and an ICC of 0.80 (range 0.58–0.94). Previous studies that investigated the MWF reproducibility reported a within-subject CoV of 19% (range 7–40%) and 12.6% (range 4.4–25.1%) for a single-slice MSE sequence (Levesque et al., 2010; Vavasour et al., 2006), while a CoV of 3.99% (range 1.77–8.93%) and ICC of 0.76 were found for a 3D MSE sequence (Meyers et al., 2013). Furthermore, in a 3D GRASE sequence a CoV of 13.2% (range 2.2–55.3%) (measured in a single subject) (Meyers et al., 2017), and an ICC of 0.83 (range 0.79–0.88) (Arshad et al., 2017) were previously reported. Hence, the multi-slice GRASE acquisition with acceleration factor 2 still provides a reproducibility that is comparable to or even better than previous studies.

While the reproducibility for the acquisition without parallel acceleration is on average slightly better compared to an acceleration factor of 2, there are no large differences in reproducibility. Therefore, the increased noise due to the parallel acquisition cannot be the determining factor that influences the reproducibility in this study. Instead, other factors such as

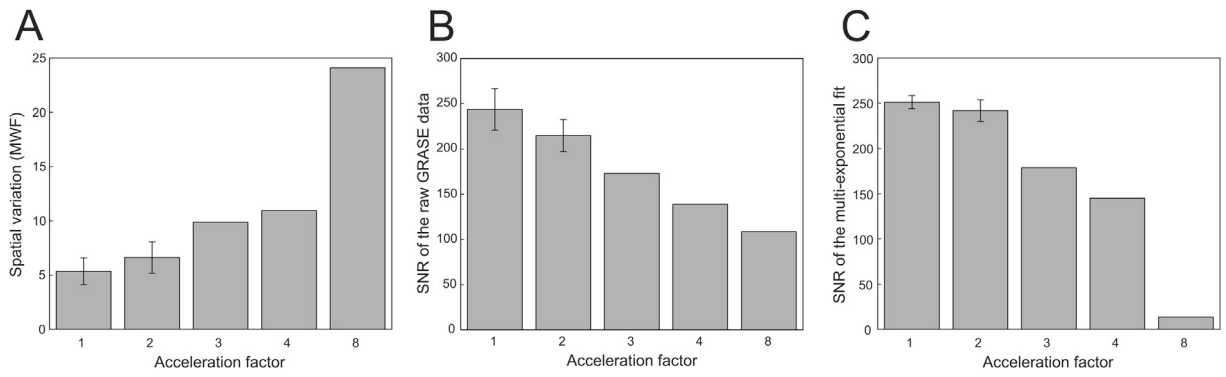

Fig. 4. A) Spatial variation of the MWF values in the splenium, B) SNR of the raw GRASE data, and C) SNR of the multi-exponential fits for varying acceleration factors. Error bars depict 1 standard error. Note that the values shown for acceleration factor 3 up to 8 are obtained in a single subject. MWF, myelin-water fraction.

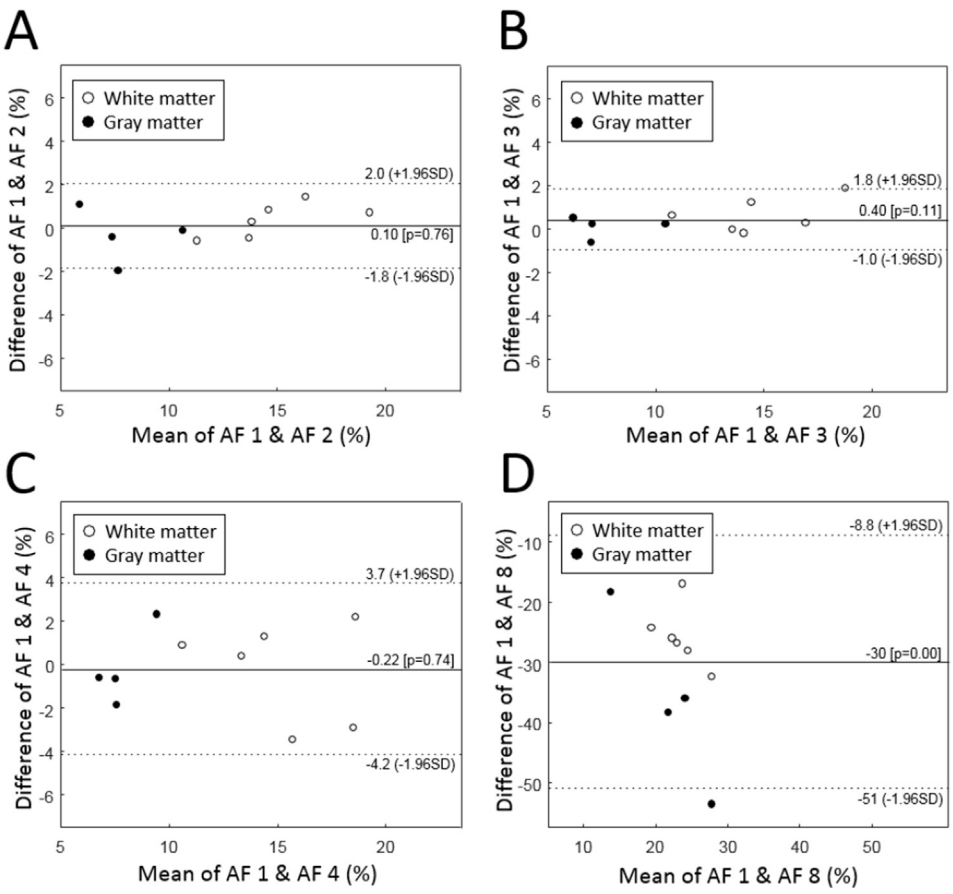

Fig. 5. Bland-Altman plots of the MWF values obtained using acceleration factor of 2 (A), 3 (B), 4 (C) and 8 (D) plotted versus the MWF values obtained with an acceleration factor of 1. The solid lines represent the bias between measurements, and the dotted lines shows the limits of agreement between the measurements. MWF, myelin-water fraction; AF, acceleration factor.

differences in slice position due to repositioning, the influence of B1 and B0 inhomogeneities, and the noise susceptible ill-posed NNLS could be important factors explaining the variation between the multi-slice scans.

4.3. Further acceleration

As expected, a higher acceleration factor leads to an increased spatial variation and decreased SNR_{raw} and SNR_{fit}. Previously, it was stated that the results from the multi-exponential fit become inaccurate when the SNR_{raw} drops below a certain threshold (approximately 100) (Meyers et al., 2009). The SNR_{raw} for acceleration factors up to 4 sufficiently fulfills this requirement, indicating that there are no major inaccuracies in the multi-exponential analysis. However, it is clearly observed that the LoA with respect to no parallel acceleration are wider for acceleration factor 4, indicating a reduced reproducibility. Interestingly, based on the LoA, an acceleration factor of 3 seems to be comparable or even better as an acceleration factor of 2, possibly indicating that these results are still reproducible. However, since these results are obtained in a single subject this conclusion cannot be drawn formally.

4.4. Clinical perspectives

Previous clinical studies investigating white matter myelin abnormalities in multiple sclerosis typically reported a difference of approximately 2–5% in absolute myelin content compared to controls (Laule et al., 2004; Vargas et al., 2015; Vavasour et al., 2006). Here we found that the average RC of the multi-slice GRASE acquisition with acceleration factor up to 2 is about 2%, indicating that such differences in myelin content can be found in 95% of the observations. Furthermore, the multi-slice acquisition is less susceptible to subject motion compared to 3D acquisition, where motion can corrupt the entire image volume. This is especially relevant in specific subject/patient groups, such as young children or patients with claustrophobic anxiety. While subject motion cannot be prevented with a 2D acquisition, it does not compromise the entire dataset.

4.5. Study considerations

In this study, the slice-profile was estimated from the slice-selective excitation pulse using a small-tip-angle approximation. While this approximation is generally considered to be a useful approximation of the Bloch equations for small flip angles (up to approximately 90°), it is not as accurate as solving the Bloch equations numerically. However, a recent study compared fitting T2 relaxation signals using the small-tip-angle approximation to numerically solving the Bloch equations, and found that in case of adequate SNR_{raw} (i.e. > 100) and a three-parameter approach (estimating T2 time, amplitude and B1 error) the small-tip-angle approximation can still provide reliable multi-exponential fits (McPhee and Wilman, 2017). Hence, we chose to employ the much less complex small-tip-angle approximation.

5. Conclusions

In this study, the applicability and reproducibility of multi-slice myelin-water imaging is evaluated. It was shown that the multi-slice GRASE images are in excellent agreement with the single slice reference method for MWF imaging, with a bias of no more than 0.9% in absolute MWF values. Furthermore, the multi-slice GRASE MWF estimation without parallel imaging acceleration and with an acceleration factor of 2

are found to be highly reproducible, with an average ICC of 0.80. Hence, a multi-slice GRASE acquisition with parallel acceleration factor 2 and a scan time of 7:30 min still provides an excellent reproducibility.

Declaration of interest

This research did not receive any specific grant from funding agencies in the public, commercial, or not-for-profit sectors.

Declaration of interest

None.

References

Akhondi-Asl, A., Afacan, O., Balasubramanian, M., Mulkern, R.V., Warfield, S.K., 2016. Fast myelin water fraction estimation using 2D multislice CPMG. Magn. Reson. Med. 76, 1301–1313. https://doi.org/10.1002/mrm.26034.

Alonso-Ortiz, E., Levesque, I.R., Pike, G.B., 2015. MRI-based myelin water imaging: a technical review. Magn. Reson. Med. 73, 70–81. https://doi.org/10.1002/mrm.25198.

Arshad, M., Stanley, J.A., Raz, N., 2017. Test-retest reliability and concurrent validity of in vivo myelin content indices: myelin water fraction and calibrated T1w/T2w image ratio. Hum. Brain Mapp. 38, 1780–1790. https://doi.org/10.1002/hbm.23481.

Bydder, M., Du, J., 2006. Noise reduction in multiple-echo data sets using singular value decomposition. Magn. Reson. Imaging 24, 849–856. https://doi.org/10.1016/j.mri.2006.03.006.

Cicchetti, D.V., 1994. Guidelines, criteria, and rules of thumb for evaluating normed and standardized assessment instruments in psychology. Psychol. Assess. 6, 284–290. https://doi.org/10.1037/1040-3590.6.4.284.

Dayan, M., Rúa, S.M.H., Monohan, E., Fujimoto, K., Pandya, S., Locastro, E.M., Vartanian, T., Nguyen, T.D., Raj, A., 2017. MRI analysis of white matter myelin water content in multiple Sclerosis : a novel approach applied to finding correlates of cortical thinning. Front. Neurosci. 11, 1–14. https://doi.org/10.3389/fnins.2017.00284.

Deoni, S.C.L., Rutt, B.K., Arun, T., Pierpaoli, C., Jones, D.K., 2008. Gleaning multicomponent T1 and T2 information from steady-state imaging data. Magn. Reson. Med. 60, 1372–1387. https://doi.org/10.1002/mrm.21704.

Faizy, T.D., Kumar, D., Broocks, G., Thaler, C., Flottmann, F., Leischner, H., Kutzner, D., Hewera, S., Dotzauer, D., Reddy, R., Fiehler, J., Sedlacik, J., Gellißen, S., 2018. Age-related measurements of the myelin water fraction derived from 3D multi-echo GRASE reflect myelin content of the cerebral white matter. Sci. Rep. 8, 1–8. https://doi.org/10.1038/s41598-018-33112-8.

Fischl, B., Dale, A.M., 2000. Measuring the thickness of the human cerebral cortex from magnetic resonance images. Proc. Natl. Acad. Sci. 97, 11050–11055. https://doi.org/10.1073/pnas.200033797.

Friston, K.J., Ashburner, J., Kiebel, S., Nichols, T., Penny, W. (Eds.), 2007. Statistical Parametric Mapping. Elsevier. https://doi.org/10.1016/B978-0-12-372560-8.X5000-1.

Glasser, M.F., Van Essen, D.C., 2011. Mapping human cortical areas in vivo based on myelin content as revealed by T1- and T2-weighted MRI. J. Neurosci. 31, 11597–11616. https://doi.org/10.1523/JNEUROSCI.2180-11.2011.

Guo, J., Ji, Q., Reddick, W.E., 2013. Multi-slice myelin water imaging for practical clinical applications at 3.0 T. Magn. Reson. Med. 70, 813–822. https://doi.org/10.1002/mrm.24527.

Hutchinson, E., Pulsipher, D., Dabbs, K., y Gutierrez, A.M., Sheth, R., Jones, J., Seidenberg, M., Meyerand, E., Hermann, B., 2010. Children with new-onset epilepsy exhibit diffusion abnormalities in cerebral white matter in the absence of volumetric differences. Epilepsy Res. 88, 208–214. https://doi.org/10.1016/j.eplepsyres.2009.11.011.

Kolind, S., Matthews, L., Johansen-berg, H., Leite, M.I., Steven, C.R., 2012. Myelin Water Imaging Reflects Clinical Variability in Multiple Sclerosis, vol. 60, pp. 263–270. https://doi.org/10.1016/j.neuroimage.2011.11.070 (Myelin).

Kumar, D., Siemonsen, S., Heesen, C., Fiehler, J., Sedlacik, J., 2016. Noise robust spatially regularized myelin water fraction mapping with the intrinsic B1-error correction based on the linearized version of the extended phase graph model. J. Magn. Reson. Imaging 43, 800–817. https://doi.org/10.1002/jmri.25078.

Laule, C., Vavasour, I.M., Kolind, S.H., Li, D.K.B., Traboulsee, T.L., Moore, G.R.W., MacKay, A.L., 2007. Magnetic resonance imaging of myelin. Neurotherapeutics 4, 460–484. https://doi.org/10.1016/j.nurt.2007.05.004.

Laule, C., Vavasour, I.M., Moore, G.R.W., Oger, J., Li, D.K.B., Paty, D.W., MacKay, A.L., 2004. Water content and myelin water fraction in multiple sclerosis. J. Neurol. 251, 284–293. https://doi.org/10.1007/s00415-004-0306-6.

Lebel, R.M., Wilman, A.H., 2010. Transverse relaxometry with stimulated echo compensation. Magn. Reson. Med. 64, 1005–1014. https://doi.org/10.1002/mrm.22487.

Leemans, A., Jeurissen, B., Sijbers, J., Jones, D., 2009. ExploreDTI: a graphical toolbox for processing, analyzing, and visualizing diffusion MR data. Proc. 17th Sci. Meet. Int. Soc. Magn. Reson. Med. 17, 3537.

Levesque, I.R., Chia, C.L.L., Pike, G.B., 2010. Reproducibility of in vivo magnetic resonance imaging-based measurement of myelin water. J. Magn. Reson. Imaging 32, 60–68. https://doi.org/10.1002/jmri.22170.

Ljungberg, E., Vavasour, I., Tam, R., Yoo, Y., Rauscher, A., Li, D.K.B., Traboulsee, A., MacKay, A., Kolind, S., 2017. Rapid myelin water imaging in human cervical spinal cord. Magn. Reson. Med. 78, 1482–1487. https://doi.org/10.1002/mrm.26551.

Mackay, A., Whittall, K., Adler, J., Li, D., Paty, D., Graeb, D., 1994. In vivo visualization of myelin water in brain by magnetic resonance. Magn. Reson. Med. 31, 673–677. https://doi.org/10.1002/mrm.1910310614.

Macmillan, E.L., Mädler, B., Fichtner, N., Dvorak, M.F., Li, D.K.B., Curt, A., Mackay, A.L., 2011. Myelin water and T 2 relaxation measurements in the healthy cervical spinal cord at 3 . 0T : repeatability and changes with age. Neuroimage 54, 1083–1090. https://doi.org/10.1016/j.neuroimage.2010.08.076.

McPhee, K.C., Wilman, A.H., 2017. Transverse relaxation and flip angle mapping: evaluation of simultaneous and independent methods using multiple spin echoes. Magn. Reson. Med. 77, 2057–2065. https://doi.org/10.1002/mrm.26285.

Meyers, S.M., Kolind, S.H., MacKay, A.L., 2017. Simultaneous measurement of total water content and myelin water fraction in brain at 3 T using a T2 relaxation based method. Magn. Reson. Imaging 37, 187–194. https://doi.org/10.1016/j.mri.2016.12.001.

Meyers, S.M., Laule, C., Vavasour, I.M., Kolind, S.H., Mädler, B., Tam, R., Traboulsee, A.L., Lee, J., Li, D.K.B., MacKay, A.L., 2009. Reproducibility of myelin water fraction analysis: a comparison of region of interest and voxel-based analysis methods. Magn. Reson. Imaging 27, 1096–1103. https://doi.org/10.1016/j.mri.2009.02.001.

Meyers, S.M., Vavasour, I.M., Mädler, B., Harris, T., Fu, E., Li, D.K.B., Traboulsee, A.L., MacKay, A.L., Laule, C., 2013. Multicenter measurements of myelin water fraction and geometric mean T 2 : intra- and intersite reproducibility. J. Magn. Reson. Imaging 38, 1445–1453. https://doi.org/10.1002/jmri.24106.

Nave, K., Werner, H.B., 2014. Myelination of the nervous system: mechanisms and functions. Annu. Rev. Cell Dev. Biol. 30, 503–533. https://doi.org/10.1146/annurev-cellbio-100913-013101.

Nguyen, T.D., Deh, K., Monohan, E., Pandya, S., Spincemaille, P., Raj, A., Wang, Y., Gauthier, S. a., 2016. Feasibility and reproducibility of whole brain myelin water mapping in 4 minutes using fast acquisition with spiral trajectory and adiabatic T2prep (FAST-T2) at 3T. Magn. Reson. Med. 76, 456–465. https://doi.org/10.1002/mrm.25877.

Ocklenburg, S., Anderson, C., Gerding, W.M., Fraenz, C., Schlüter, C., Friedrich, P., Raane, M., Mädler, B., Schlaffke, L., Arning, L., Epplen, J.T., Güntürkün, O., Beste, C., Genç, E., 2018. Myelin water fraction imaging reveals hemispheric asymmetries in human white matter that are associated with genetic variation in PLP1. Mol. Neurobiol. https://doi.org/10.1007/s12035-018-1351-y.

Petrovic, A., Scheurer, E., Stollberger, R., 2015. Closed-form solution for T2 mapping with nonideal refocusing of slice selective CPMG sequences. Magn. Reson. Med. 73, 818–827. https://doi.org/10.1002/mrm.25170.

Prasloski, T., Rauscher, A., MacKay, A.L., Hodgson, M., Vavasour, I.M., Laule, C., Mädler, B., 2012. Rapid whole cerebrum myelin water imaging using a 3D GRASE sequence. Neuroimage 63, 533–539. https://doi.org/10.1016/j.neuroimage.2012.06.064.

Seifert, A.C., Li, C., Wilhelm, M.J., Wehrli, S.L., Wehrli, F.W., 2017. Towards quantification of myelin by solid-state MRI of the lipid matrix protons. Neuroimage 163, 358–367. https://doi.org/10.1016/j.neuroimage.2017.09.054.

Sheth, V., Shao, H., Chen, J., Vandenberg, S., Corey-Bloom, J., Bydder, G.M., Du, J., 2016. Magnetic resonance imaging of myelin using ultrashort Echo time (UTE) pulse sequences: phantom, specimen, volunteer and multiple sclerosis patient studies. Neuroimage 136, 37–44. https://doi.org/10.1016/j.neuroimage.2016.05.012.

Skinner, M.G., Kolind, S.H., MacKay, A.L., 2007. The effect of varying echo spacing within a multiecho acquisition: better characterization of long T2 components. Magn. Reson. Imaging 25, 840–847. https://doi.org/10.1016/j.mri.2006.09.046.

Uddin, M.N., Figley, T.D., Marrie, R.A., Figley, C.R., 2018a. Can T1w/T2w ratio be used as a myelin-specific measure in subcortical structures? Comparisons between FSE-based T1w/T2w ratios, GRASE-based T 1 w/T 2 w ratios and multi-echo GRASE-based myelin water fractions. NMR Biomed. 31, e3868. https://doi.org/10.1002/nbm.3868.

Uddin, M.N., Figley, T.D., Figley, C.R., 2018b. Effect of echo time and T 2 -weighting on GRASE-based T 1 w/T 2 w ratio measurements at 3T. Magn. Reson. Imaging 51, 35–43. https://doi.org/10.1016/j.mri.2018.04.012.

van Buchem, M.A., Steens, S.C., Vrooman, H.A., Zwinderman, A.H., McGowan, J.C., Rassek, M., Engelbrecht, V., 2001. Global estimation of myelination in the developing brain on the basis of magnetization transfer imaging: a preliminary study. AJNR. Am. J. Neuroradiol. 22, 762–766.

Vargas, W.S., Monohan, E., Pandya, S., Raj, A., Vartanian, T., Nguyen, T.D., Hurtado Rúa, S.M., Gauthier, S.A., 2015. Measuring longitudinal myelin water fraction in new multiple sclerosis lesions. NeuroImage Clin 9, 369–375. https://doi.org/10.1016/j.nicl.2015.09.003.

Vavasour, I.M., Clark, C.M., Li, D.K.B., MacKay, A.L., 2006. Reproducibility and reliability of MR measurements in white matter: clinical implications. Neuroimage 32, 637–642. https://doi.org/10.1016/j.neuroimage.2006.03.036.

Vavasour, I.M., Whittall, K.P., Li, D.K.B., Mackay, A.L., 2000. Different magnetization transfer effects exhibited by the short and long T 2 components in human. Brain 866, 860–866.

Whittall, K.P., MacKay, A.L., 1989. Quantitative interpretation of NMR relaxation data. J. Magn. Reson. 84, 134–152. https://doi.org/10.1016/0022-2364(89)90011-5.

Wong, S.M., Backes, W.H., Zhang, C.E., Staals, J., van Oostenbrugge, R.J., Jeukens, C.R.L.P.N., Jansen, J.F.A., 2018. On the reproducibility of inversion recovery intravoxel incoherent motion imaging in cerebrovascular disease. Am. J. Neuroradiol. 39, 226–231. https://doi.org/10.3174/ajnr.A5474.

Wu, B., Wang, C., Pang, Y., Zhang, X., 2010. Comparison of SNR calculation methods for in vivo imaging. In: Proc. Intl. Soc. Mag. Reson. Med., p. 3153.